Implementation of forward osmosis to concentrate alpha-ketoglutaric acid from fermentation broth: Performance and fouling analysis

Mateusz Szczygiełda[a], Martyna Krajewska[a], Lei Zheng[b, c], Long D. Nghiem[c], Krystyna Prochaska[a]

[a] Institute of Chemical Technology and Engineering, Poznan University of Technology, Berdychowo 4, 60-965 Poznań, Poland

[b] Chongqing Institute of Green and Intelligent Technology, Chinese Academy of Sciences, Chongqing 400714, China

[c] Centre for Technology in Water and Wastewater, University of Technology Sydney, Ultimo, NSW 2007, Australia

*Corresponding author: krystyna.prochaska@put.poznan.pl

Graphical abstract:

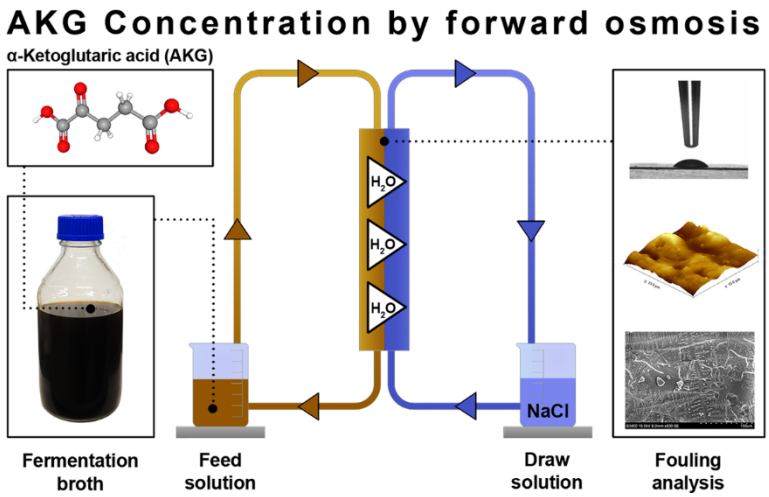

Abstract

Forward osmosis (FO) was demonstrated as a promising method to concentrate alpha-ketoglutaric acid in fermentation broth. Using a model solution containing alpha-ketoglutaric acid, the impact of the initial pH value on water flux, reverse salt flux, and rejection of alpha-ketoglutaric acid were first elucidated. Results from this study show that water flux was not affected by feed solution pH. However, feed solution pH could influence alpha-ketoglutaric acid rejection and reverse salt flux. The highest alpha-ketoglutaric acid rejection of 99.7% and lowest reverse salt flux were observed at pH 5. Multi-component model and real fermentation broth were then used to validate FO application for concentrating alpha-ketoglutaric acid. Water recovery of 80% was achieved without severe membrane fouling. In addition, membrane fouling analysis show that the built-up fouling layer of impurities is flaky and of unstable nature, suggesting that membrane fouling could be reversible. Knowledge of the fouling layer formation can contribute to the development of an effective method of pretreatment of the fermentation broth and cleaning FO membranes in the future.

Keyword: forward osmosis, alpha-ketoglutaric acid, membrane fouling, fermentation broth.

1. Introduction

Alpha-ketoglutaric acid (AKG) is a biological compound found naturally in the human body. It plays an important role in the tricarboxylic acid cycle to release stored energy to the body [1,2]. AKG cannot be obtained from food. It can only be synthesized from non-essential amino acids from the body or obtained as a supplement usually in the form of tablets. AKG has many demonstrated health benefits as a nutraceutical and medicine [3]. For example, AKG can be orally administered to treat cyanide poisoning [4], control and prevent oxidative stress [5,6], and improve immune regulation [7]. AKG can also be used as a nutritional supplement to support skeletal development in adolescents, inhibit the process of osteoporosis in women, increase muscle mass, and accelerate wound healing process [8]. Recent literature has suggested the potential of AKG as a substrate in thermal polycondensation reaction to an elastomer (i.e. poly (triol α-ketoglutarate)) [9] and in the synthesis of new N-heterocyclic biochemicals for cancer treatment [10].

At industrial scale, AKG is produced from diethyl succinic and oxalic acid esters using multi-stage chemical synthesis [11]. Chemical synthesis of AKG is not efficient (approximately 75% efficiency) and generates a large amount of copper catalyst hazardous waste [11]. An

environmentally friendly alternative to chemical synthesis is microbiological production of AKG using bacteria (i.e. *Arthrobacter paraffineus*, *Pseudomonas fluorescens*, *Serratiamarcescens*) and *Yarrowia Lipolytica* yeast [11,12]. This microbiological process produces AKG in a multi-component mixture (called post-fermentation broth), containing the unreacted substrates, biomass, sugars, polyols and inorganic salts [13]. Of a particular note, AKG concentration in the fermentation broth is usually less than 10%. Thus, a major cost component (50-80%) of microbiological production is associated with the separation, concentration, and purification of AKG from the fermentation broth [14].

Current methods for the separation and concentration of the carboxylic acids from fermentation broth include distillation, vacuum evaporation, solvent extraction, ion exchange, and precipitation [15–17]. These methods consume a large volume of often hazardous solvents are energy intensive. Thus, there have been several recent scientific investigations to apply membrane separation techniques, including microfiltration (MF), ultrafiltration (UF), nanofiltration (NF), reverse osmosis (RO), classical electrodialysis (ED), and bipolar membrane electrodialysis (EDBM) to reduce the cost and environmental impact of AKG production [18–22]. In a previous work, we have demonstrated a hybrid process to separate AKG from fermentation broth. Our hybrid process consisted by a multi-stage system (centrifugation - UF - NF - EDBM - vacuum evaporation - crystallization) to obtain AKG with purity of 95% that is required for industrial application [13]. However, energy consumption for AKG separation remains high due to the vacuum evaporation step in this hybrid system.

Forward osmosis is an emerging membrane separation process ideal for the separation of complex and challenging solutions. In the FO process, water is transported across a semi-permeable membrane by an osmotic gradient between the feed solution and a concentrated salt solution, commonly known as the draw solution. Because the FO process is driven by the osmotic potential, it does not require any external energy input apart from a small amount of energy for circulating the feed and draw solutions. The absence of an external hydraulic pressure makes the FO process more attractive due to low fouling propensity and easy fouling reversibility. FO applications for concentrating a wide range of challenging solutions for food processing such as juice and fermentation broth, and industrial wastewater treatment such as sludge and drilling fluid [25–29]. ~~In the FO process, water is transported across a semi-permeable membrane by an osmotic gradient between the feed solution (FS) and the draw solution (DS) [30]. FO is a low-energy-consuming alternative contrast to classical concentration methods (evaporation/distillation) [24].~~ FO has also been proposed as an

alternative for the separation and concentration of organic acids, including succinic, acetic, propionic, and lactic acid from fermentation broth [29,31,32].

An exemplary concept of the concentration of succinates from the post-fermentation broth in the NF-FO hybrid system was reported by Law and Mohammad [33]. The proposed concept assumed the simultaneous concentration of succinic acid and application waste byproduct stream (consisting of organic salts such as sodium acetate and sodium formate from the broth) as DS. Law and Mohammad [33] reported a high rejection of succinate of over 99% by a cellulose triacetate FO membrane. In another work, Law et al., [29] presented a new method for succinic acid separation in a sequential hybrid system, which combines the FO process with other traditional separation techniques, to obtain high purity product of 90.5%. Apart from previous investigations by Law and co-workers, there are no reports in the literature to evaluate the potential of FO to concentrate water fermentation broth of keto-acids.

Previous literature suggests that the efficiency of concentrating carboxylic acids in the FO process is dependent on the pH and composition of the feed solution (FS) [29,34]. The dissociation of carboxylic and keto-carboxylic acids is governed by pH of the feed solution. Organic acid speciation is a key parameter that determines their rejection by the FO membrane. The rejection mechanism of AKG by FO membranes may differ from that of simple organic acids such as succinic acid, due to their different molecular weights and physicochemical properties. Fouling phenomena is usually considered as the main hindrance in the implementation of the membrane technologies, which is especially pronounced in the case of separation of the actual post-fermentation broths. Despite the FO operates without hydraulic pressure, which makes the membrane less prone to blockage than in pressure-driven techniques, due to the composition complexity of the fermentation broth, there is still a high risk of a decrease in the efficiency of the separation process. Therefore, the fouling layer analysis could contribute to the development of an effective method of pre-treatment of the fermentation broth and an effective way of cleaning FO membranes [35].

This study aims to elucidate, for the first time, the impact of initial pH of FS on extraction of AKG from fermentation broth. The efficiency of AKG concentration from a single and multi-component model solutions and real fermentation broth will be compared. The interplay between fouling and separation performance is elucidated to provide further insight for scaling up.

2. Materials and methods

2.1. FO membrane

A flat-sheet cellulose triacetate (CTA) membrane (FTSH2O, Fluid Technology Solutions, US) was used for FO process. This CTA membrane is composed of a thin cellulose triacetate active layer formed on the support layer of an embedded woven polyester mesh. This cellulose triacetate is highly resistant to hydrolysis; thus, it can be operated at pH values in the range of pH 3 to 8. Additional information about this membrane is available in the Supplementary Information.

2.2. Draw and feed solutions

All chemicals and reagents used in this study were of analytical grade, unless otherwise specified. Sodium chloride (NaCl) purchased from CHEMPUR (Poland) was used as the DS. AKG, lactic acid (LA), acetic acid (AA) (Sigma-Aldrich, Poland), and ethanol (POCH, Poland) were selected as the model organic compounds to represent the major compounds of post-fermentation broth in this study. A single component and multi-component model solutions were prepared adding AKG (10 g/L) and a mixture of AKG (10 g/L), LA (12.3 g/L), AA (2.4 g/L) and ethanol (13.2 g/L) to deionized (DI) water, respectively. According to the literature, these value are representative concentrations of organic compounds in fermentation broth [34]. Fermentation broth was also obtained from a mixed culture of *Bacillus natto* and *Pseudomonas fluorescens* (Poznan University of Life Sciences [10]) and used in this study. This fermentation broth was pretreated by centrifugation and vacuum filtration to remove suspended solids. The total protein concentration (N × 6.25) in the fermentation broth was 1.2 g/L as measured by the Kjeldahl method (PN-A04018:1975). The pH of the FS was adjusted by the addition of pure NaOH microgranules (CHEMPUR, Poland) to the water solutions of AKG while mixing. DI with a conductivity not exceeding 3 μS/cm was used to prepare all working solutions.

2.3. FO experiment protocol

All experiments were carried out using a lab-scale FO setup (Fig. 1) equipped with a membrane module consisting of two identical and symmetrical plastic flow chambers with length 14 cm, width 8 cm and height 1 cm, and (corresponding effective internal area 32 cm^2).

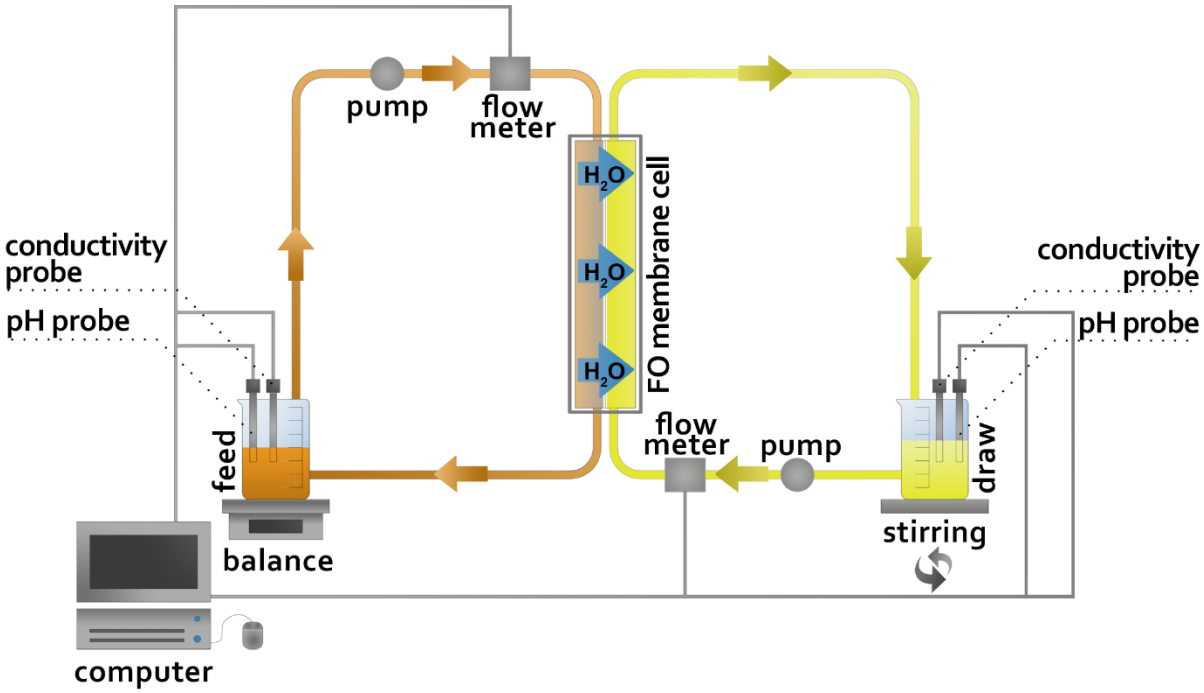

Fig. 1. A schematic diagram of a lab-scale FO setup.

DI water, model solution, and fermentation broth were used as the FS with the volume of 0.3 L. NaCl (3 M) was used as the DS with the volume of 0.4 L. The selected concentration of DS is within the range of NaCl solubility in water (6.14 M) and it could generate sufficient osmotic pressure (136.68 bar) with limited reverse salt flux. The system was operated in the (counter-current) FO configuration with the active layer facing feed solution (AL-FS) orientation. Before target FO process (model or real broth), baseline test was carried out using the same experimental conditions (DI water as FS). Feed and draw solutions were recirculated at a constant flow rate 0.7 L/min (corresponding to a cross flow velocity 0.03 m/s). The feed reservoir was placed on a digital balance (Radwag, Poland) and its weight change was recorded every 60 s to measure the change of water flux. pH, ~~and~~ conductivity and temperature of feed and draw solution were monitored by a conductivity, ~~and~~ pH and temperature probe (Elmetron, Poland) every 60 s. During all FO experiments, the operating temperature (T) was kept at 23 ± 1 °C.

All experiments were conducted in duplicate. Each experiment was conducted over 120 min (section 4.1) or until 80% water recovery from feed reservoir (section 4.2) has been achieved. Samples of feed and draw solutions (1.5 mL) were taken at the beginning and end of each experiment as well as at fixed intervals for analysis. Water flux (J_w) was calculated as:

$$J_w = \frac{\Delta m}{\rho \times A_m \times \Delta t} \quad (1)$$

where J_w represents water flux, L/m^2·h; Δm denotes mass variation of FS over a time interval of Δt, g; ρ represents water density, g/L; A_m is the effective membrane area, m^2 ; Δt is time interval, h.

The reverse salt flux (J_s) was calculated based on a mass balance calculation as:

$$J_s = \frac{(C_t \times V_{feed,t} - C_0 \times V_{feed,0})}{A_m \times t} \quad (2)$$

$$V_{feed,t} = V_{feed,0} - \Delta V_{p,t} \quad (3)$$

where C_0 and C_t represent the concentration of the draw solute in the FS at the beginning and corresponding time t of the experiment, mol/L; $V_{feed,0}$ and $V_{feed,t}$ represents the volumes of the feed at the beginning and corresponding time t of the experiments, L; $\Delta V_{p,t}$ is the volume of permeate at the time t, L.

Water recovery (R_w, %) of FO experiment is defined as the volume fraction of feed that recovered as the permeate:

$$R_w = \frac{Q_p}{Q_F} \quad (4)$$

where Q_p represents the volume of transferred water, Q_F denotes the volume of FS.

The dilution factor (DF) was defined as:

$$DF = \frac{V_d}{V_p} \quad (5)$$

where DF denotes the dilution factor; V_d represents the final volume of the DS, L; V_p represents the total volume of permeate, L.

The rejection ratio (R) was calculated as:

$$R = (1 - \frac{DF \times C_{draw}}{C_{feed}}) \times 100\% \quad (6)$$

where R stands for the rejection ratio; C_{draw} denotes the concentration of each organic acid in the DS, g/L; C_{feed} represents the concentration of each organic acid in the FS, g/L.

The flux decline (FD) was calculated as:

$$FD = (1 - \frac{Jw(t)}{Jw(0)}) \times 100\% \quad (7)$$

where FD represents the flux decline, %; $J_{w(0)}$ stands for the water flux at the beginning of the experiment , L/m^2·h; $J_{w(t)}$ represents value of water flux at time t, L/m^2·h.

Concentration factor (CF) was calculated as:

$$CF = \frac{C_{AKG(t)}}{C_{AKG(0)}} \quad (8)$$

where CF represents the concentration factor; $C_{AKG(0)}$ denotes the initial concentration of AKG in FS, g/L; $C_{AKG(t)}$ denotes the final concentration of AKG in FS, g/L.

2.4. Analytical methods

2.4.1. Surface morphology analysis

The pristine membrane was conditioned in water and further allowed to dry for at least 48 h before measurement. The fouled FO membrane was also allowed to dry for two days prior to analysis. Prior to scanning electron microscopic (SEM) analysis, membrane samples were sputtered with carbon using a Cressington Carbon Coater 108carbon/A. They were subsequently analyzed (both qualitatively and quantitatively) by the Thermo Scientific NSS spectral imaging system (coupled with scanning electron microscope, SEM) for the Energy Dispersive X-ray Spectrometry technique (EDS). The SEM (S-3400N Hitachi) was used to observe surfaces and cross-sections of samples. Secondary electron detectors were used in SEM and EDS modes.

The topography analyses of clean and fouled membranes were conducted using the atomic force microscope (AFM) NX10 (Park Systems, Korea). A fresh AFM cantilever (All-In-One D, Budget Sensors, Bulgaria) was used for each sample to avoid contamination. A nominal force constant was about 40 N/m. The measurements were operated in the non-contact mode with a resolution of 512 pixels in an ambient environment (room temperature 22 ^{o}C). The scanning speed was ranged from 0.3 to 0.5 Hz (depending on the scanning size). In addition to the topographical measurements, the mean roughness data (Ra) were extracted for each membrane sample from a 10 × 10 μm^2 scanning area. The uncertainty was obtained from the standard deviation of at least five individual measurements. All atomic force microscopy data were processed with Gwyddion software.

2.4.2. Membrane Wettability and Surface Free Energy

Contact angle measurements were performed on the air-dried pristine and fouled membranes by a Theta Lite device (Biolin Scientific, Finland) controlled by the One Attension software. The contact angles were measured by releasing a microdroplet of 2 µL ultrapure water (18 MΩ·cm, pH 6.20) onto the membrane surface. The drop shape was recorded by a digital camera to determine the average value from right and left-side angles. At least 10 independent measurements were performed on each sample. The van Oss-Chaudhury-Good method – vOCG (equations 9 and 10) was applied to measure the surface free energy by using ultrapure water and formamide (as polar liquids) and diiodomethane (as an apolar liquid). vOCG approach defines the surface free energy as the sum of short-range acid−base interactions and long-range Lifshitz-van der Waals interactions.

$$\gamma = \gamma^{LW} + \gamma^{AB} = \gamma^{LW} + 2\sqrt{\gamma^{+}\gamma^{-}} \tag{9}$$

$$(1 + cos\theta_i)\gamma_{li} = 2\left(\sqrt{\gamma_{li}^{LW}\gamma_s^{LW}} + \sqrt{\gamma_{li}^{+}\gamma_s^{-}} + \sqrt{\gamma_{li}^{-}\gamma_s^{+}}\right) \tag{10}$$

In the above equations, θ is the measured contact angle for a given liquid, *LW* represents the Lifschitz-van der Waals component of the surface tension, *AB* is the acid-base component, γ^{+} denotes the electron acceptor component and γ^{-} denotes the electron donor component, γ_{li} and γ_s stand for the liquid and solid phase of liquid.

2.4.3. Organic compound analysis

All collected samples were analyzed by using a high-performance liquid chromatography (HPLC) HP Agilent 1100 Series (Germany). Detailed information on the analytical method is available in our previous work [13].

2.4.4. Chloride analysis

The chloride amount in the sample was determined by using potentiometric titration with a titrator 703 Ti Stand (Metrohm, Poland). In each analysis, 10 mL of water and 1 mL of acetate buffer (pH about 2) were added to 5 mL of the sample (DS or FS) and titrated with 0.1 N

$AgNO_3$ solution until AgCl was completely precipitated. The concentration of chloride anions was calculated by:

$$C_{Cl^-} = \frac{C_{AgNO3} \cdot V_{AgNO3}}{V_{sample}} \quad (11)$$

where C_{Cl^-} stands for the concentration of chloride ions in FS or DS, mol/L; C_{AgNO_3} is the concentration of titrant $AgNO_3$, mol; V_{AgNO_3} is the volume of titrant $AgNO_3$, mL; V_{sample} represents the volume of sample used for analysis, mL.

3. Results and discussion

3.1. Impact of initial pH of one-component model solution of AKG

In the range of pH 3 to pH 5, the pH of FS did not show any observable impact on water flux (Fig. 2). The CTA membrane used in this study has a low surface charge density. Thus, pH is not expected to significantly affect water flux. This observation is in contrast to an earlier study by Jung et al., (2015), who reported decrease of water flux in the range of pH 3 to 8 when they used CTA FO membrane to extract succinic acid, ethanol, and a mixture of acetone–butanol–ethanol from simulated fermentation broths [36]. However, the change in the water flux in the pH range from 4 to 8 was insignificant and ranged from 11.80 to 11.08 $L/m^2 \cdot h$.

AKG is a weak organic acid with two acidic constants (pKa_1: 2.5; pKa_2: 4.7) [22]. Thus, AKG exists as an anionic form (AKG^- or AKG^{2-}) in acidic condition at pH 3 or above. As the solution pH increases to pH 5, the speciation of AKG moves towards AKG^{2-} (Fig. SM1). Thus, that regardless of the initial pH of the FS osmotic pressure gradient across the membrane in the FO time considered is comparable.

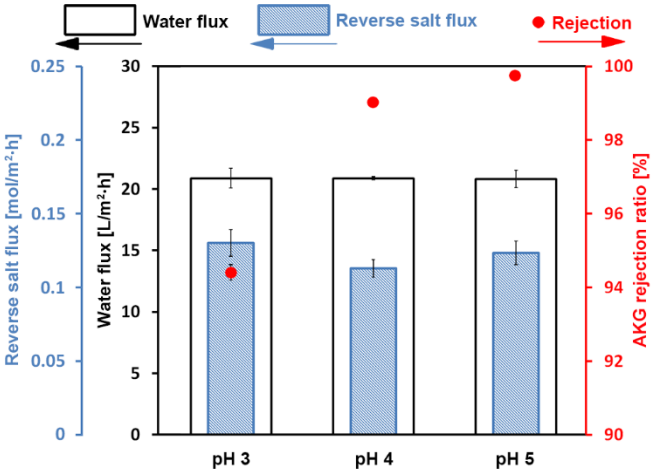

Fig. 2. Water flux, reverse salt flux and AKG rejection at different initial pH of one-component model solution over 120 min of the FO process (V_{draw} = 0.4 L; V_{feed} = 0.3 L; T = 23 ± 1 °C).

AKG rejection was above 94% at pH 3 and increased further to 94.4% and 99.7% at pH 4 and pH 5, respectively. The strength of electrostatic interactions increases with the increase of ionization: AKG <AKG^-<AKG^{2-} [13]. Similar effects were observed by Law et al. (2018) [34] during the FO process of succinic acid. However, the degree of AKG rejection in the FO process of solutions with a low initial pH of 3 is greater than succinic acid due to a larger molecular weight (146.11 Da) and greater degree of dissociation. The rejection of ionic components by FO membrane can be explained by two mechanisms: the sieve effect and electrostatic interaction between the dissolved substance and the negatively charged active layer of CTA FO membrane [29].

Some variation of RSF in the range from (0.105 to 0.131 mol/m^2·h) was observed in Fig. 2. It appears that for a small mobile solute with a high diffusion coefficient, the initial DS concentration has a higher impact than that of initial pH of feed solution on the RSF. A consequence of the reverse permeation of the solute through the FO membrane is to reduce the osmotic pressure gradient across the membrane [29]. Based on the results in Fig. 2, FS at pH 5 was used for the further testing.

3.2. **Concentration of AKG from model and real fermentation broth**

The water fluxes as a function of water recovery for different FS are shown in Fig. 3. The initial water flux (calculated after 1% of water recovery) decreased in the following order: baseline (24.2 L/m^2·h) > one-component solution (23.4 L/m^2·h) > model broth (16.5 L/m^2·h) > fermentation broth (14.4 L/m^2·h). According to the van't Hoff equation, greater number of components in the FS generates the larger osmotic pressure, thus, shrinking the effective net driving force between FS and DS [37]. Of a particular note, a decrease in the initial water flux value (approx. 41% flux loss) compared to the baseline was noticed for the fermentation broth due to the complex nature of this mixture (e.g., inorganic ions, color impurities etc.). Moreover, the water flux consistently decreases as a function of water recovery.

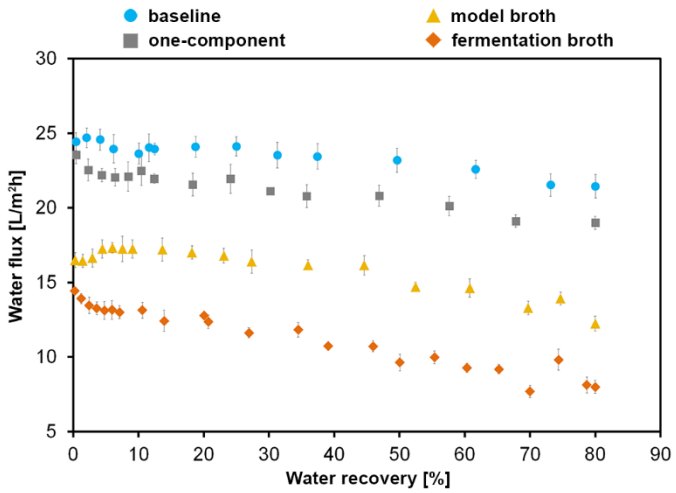

Fig. 3. Water flux in FO processes using different type of feed solution (V_{draw} = 0.4 L; V_{feed} = 0.3 L; T = 23 ± 1 °C).

Flux decline of 12% after 80% water recovery in the baseline (Fig.3) was due to the dilution effect in the DS. On the other hand, the flux decline calculated for the FO process of a one-component solution, model broth, and fermentation broth was significantly larger at 18.5, 26.1, and 44.4%, respectively. In this case, an additional effect was observed related to the cake-enhanced osmotic pressure phenomenon within the fouling layer and the increasing solute concentration in the FS as a function of water recovery. The cake-enhanced osmotic pressure phenomenon was first systematically revealed and described by Lee et al. Within the fouling layer, osmotic pressure on the feed side is higher than the bulk solution. In other words, the actual osmotic gradient or the driving force for water permeation is smaller due to the cake later. The gradual increase in AKG and salt concentration in the feed also leads to flux decline. The concentration of AKG increased as a function of water recovery from the 10 to 20 g/L at the end of the FO process (Fig. 4). Although the final flux of 8 L/m^2·h at the FO process with fermentation broth was much lower compared to the final flux in the baseline process of 21.4 L/m^2·h (Fig. 3), a high degree of water recovery was achieved.

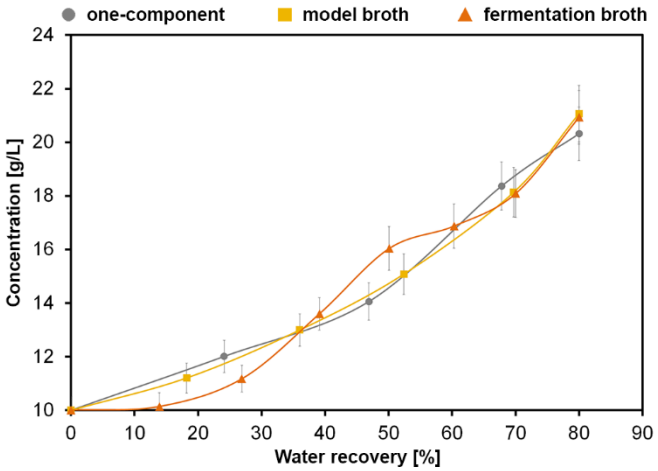

Fig. 4. Change of AKG concentration during FO processes using different type of feed solution (V_{draw} = 0.4 L; V_{feed} = 0.3 L; T = 23 ± 1 °C).

High AKG retention rates in the range of 96 - 98% (Fig. 5) were achieved in all FO tests (for different FS but constant initial pH equal to 5). However, these values are slightly lower than the results presented in section 4.2 for the process where the initial pH of FS was equal to 5 (R = 99.7%). The lower retention rate in the FO processes carried out until 80% of water recovery is a consequence of increased alpha-ketoglutarate permeation from the FS to the DS. A possible reason for this effect may be the intensification of a phenomenon known as external concentration polarization [38]. As the water recovery increased, the concentration of AKG in the FS increased significantly (Fig. 4), which spontaneously led to an increase in the accumulation of alpha-ketoglutarates directly on the membrane surface [33]. On the other hand, the progressive dilution of the DS and the increased reverse migration of alpha-ketoglutarate may limit the counter-current salt diffusion. As shown in Fig. 5, the calculated values of RSF for each FO process were relatively low and in the range from 0.05 to 0.08 mol/m^2·h. In particular, the low RSF after the FO process of the actual post-fermentation broth may be related to the compacted cake layer formation (on the active side), which played a role of an additional physical filter and impedes the migration of the salt towards the FS.

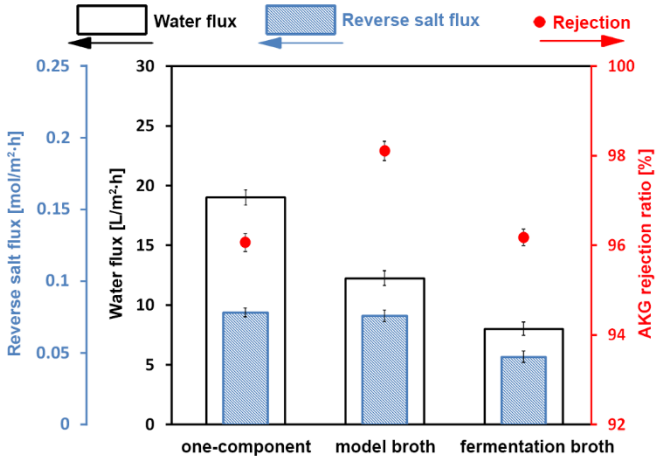

Fig. 5 Water flux, reverse salt flux and rejection of alpha-ketoglutaric acid for different type of feed solution at 80% water recovery (V_{draw} = 0.4 L; V_{feed} = 0.3 L; T = 23 ± 1 °C).

4.3 Membrane fouling by fermentation broth

4.3.1 Surface morphology and foulant composition

EDS analysis provides useful information about the surface elemental composition. The main constituents of the surface of the pristine membrane (on both the active and supporting layer) were carbon and oxygen (Fig. 6A and 6C), which is consistent with the chemical structure of the membrane components. After the FO process, apart from carbon and oxygen, there were also sodium, chlorine, silicon, calcium, magnesium, and potassium detected in the fouling layer (Fig. 6 B and Supplementary Information). SEM images show that the membrane surface was entirely and extensively covered with the cake layer (Fig. 6F and H). Data in Fig. 6 shows that carbon and oxygen dominating on the membrane surface after the FO process are derived from the fermentation broth residues (glucose and compounds responsible for bacterial colorization). In agreement to our work, Law et al. [29] suggested that glucose is a significant factor contributing to the formation of the cake layer in the succinic acid recovery from fermentation broth by FO. The uncharged glucose molecules could be adsorbed on the membrane surface together with a range of other impurities. The presence of a wide variety of different elements on the membrane surface reflected the complex composition of the fermentation broth (including microorganism cells, protein, and salt deposits). The occurrence of sodium and chlorine element was apparent since NaCl solution was used as the DS during the process. No other components except sodium and chlorine were detected in the supporting layer (Fig. 6D), which indicating that the FO process was undisturbed.

As illustrated in Fig. 6E and G, the clean membrane was observed with a clearly visible mesh structure. In comparison, membrane after FO process was completely covered by the

heterogeneous cake layer (Fig. 6F and H). Underneath the fouling layer, the mesh structure can only still be recognized, but also the traces of salt crystallization or even aggregated particles of salts was visible at higher magnifications. The cross-section SEM images confirmed that the fouling layer was built on the active side of the membrane (Fig. SM3). After the process, the active side of the membrane features a visible coating, which was flaky and appeared not to be compacted (which was possibly associated with the lack of pressure applied, side stream configuration of the FO module, and relatively short time of the process). It is also worth noting that the fouling was not evenly distributed on the membrane surface.

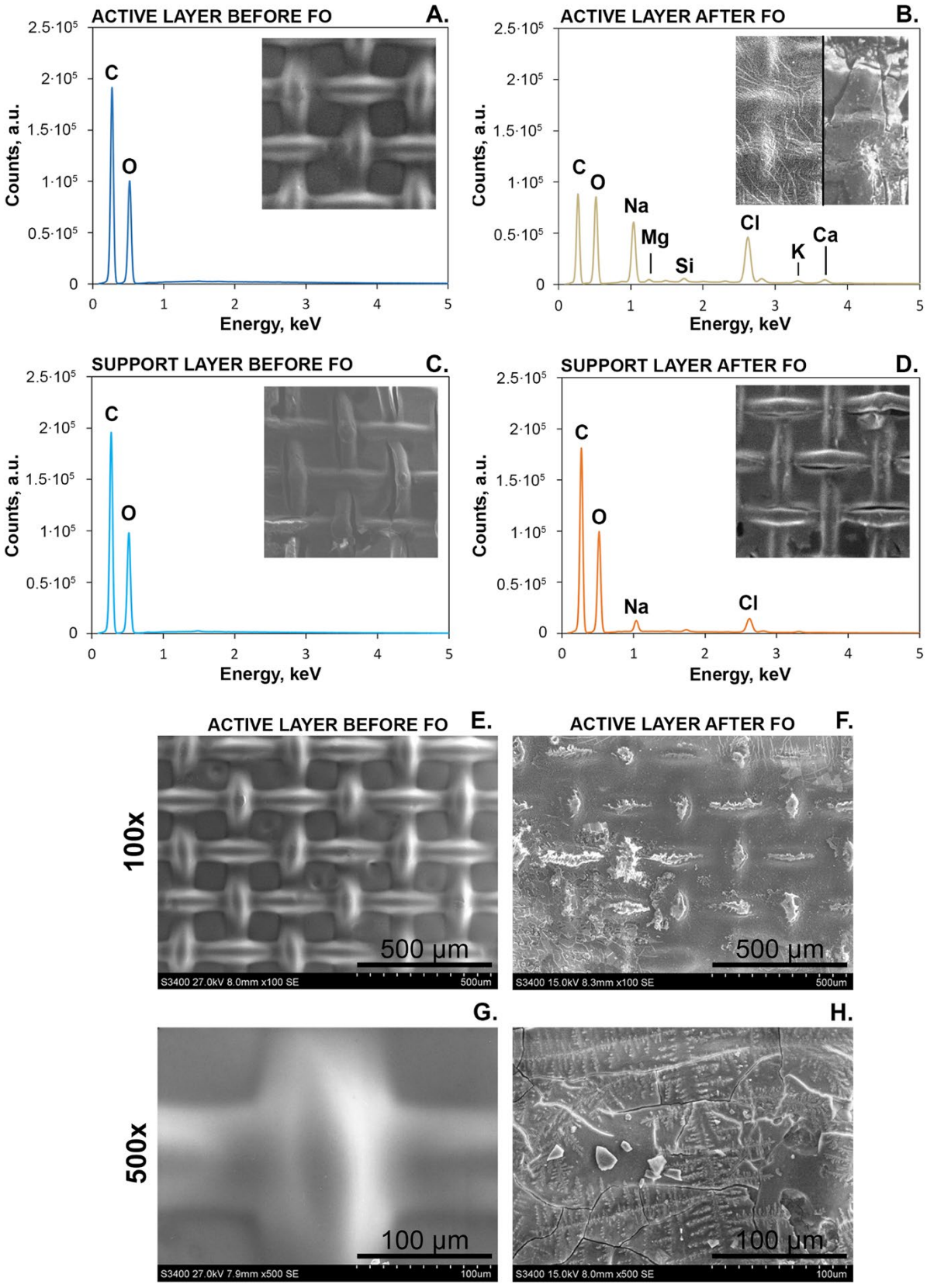

356

357 Fig.6. A-D. EDS spectra of the active and support layers of the forward osmosis CTA
358 membrane before and after the process with fermentation broth; inset SEM images of the
359 corresponding membranes for illustration purpose; E-H. SEM images of the active layer of

virgin CTA membrane (first column) and fouling cake layer (second column) at two magnifications.

Changes in thickness and morphology between the membrane before and after the process with the real fermentation broth were also visualized using atomic force microscopy (Fig. SM4). The membrane covered with the cake layer showed a much higher roughness value of 431.53 nm compared to the pristine one. The membrane thickness after the process was significantly larger and the topology of the membrane surface was apparently more diverse. According to the literature, at the micrometer scale, the impurities may deposit in the "valleys" rather than on the "hills" of the membrane due to the microflows resulting in an uniform thickness of the membrane after FO [39].

4.3.3 Contact angles and surface free energy

Contact angle analysis provides physicochemical characteristics of the foulant layer and defines the nature of complex foulant-membrane interactions. To determine the adhesion of foulants to the membrane surface, the hydrophobicity was characterized by measuring the contact angles of both sides of the membrane before and after the FO process. The contact angles of the hydrated membrane were 64.23° ± 1.53° and 66.28° ± 1.94° for the active and support layer respectively, which were moderately hydrophilic. These results concurred with other studies for similar membrane materials [27, 38]. It should be noted that the values of contact angles of the dry membranes may give an over-estimated result since the membrane normally operated when hydrated [41].

The surface free energy was determined to investigate the mechanism of non-covalent interactions between membrane and foulant. Table 1 presents the values of surface free energy calculated by the van Oss-Chaudhury-Good approach based on the contact angles measured on dried membranes. The pristine membrane demonstrated similar characteristics for both active and supporting layers, which was considered to be of relatively low surface free energy (γ^{TOT}=30.52 and 35.41 mJ/m^2 for active and support layers respectively). As a result of the deposition of organic foulants altering the membrane surface, the total surface free energy of both sides of the membrane increased slightly after the FO process. For the active layer, the value of the γ^{AB} component (describing acid-base interactions) increased significantly, while the Lifshitz-van der Waals component decreased. Such a phenomenon was not observed on the supporting layer. Thus, it indicated that the significance of the Lewis acid–base interactions (of short-range, mainly hydrogen bonds) increased in comparison with the pristine membrane surface. It is also worth noting that the γ^- component of fouled membranes (active and

supporting layer) exhibited a significantly higher value than the γ^+ component after FO process, thus, the membrane surface was of high electron donor character [42,43]. All membrane samples exhibit non-polar property. The γ^- values of the membrane depend on the surface chemistry. Among the fouling layer, each component contributes to an increase in complexity of the physiochemical mechanisms and causes the presence of lone pairs of electrons resulting in high electron-donicity tuning the surface property.

The membrane-foulant interaction influenced the formation of the initial fouling layer. As the separation process continues, the interactions between fouling components govern the long-term fouling formation [41]. The values of the surface free energy components of a clean membrane and a membrane covered with a fouling cake layer differ significantly, which indicates a miscellaneous mechanism of interaction on the surface. In the perspective of longer processes, this will impact the formation of membrane-foulant interactions in the initial stage and foulant-foulant in the further stage of the process. In the case of the analysis of such a complex medium as the actual post-fermentation broth (especially after limited pretreatment), it is an intricate process.

Table 1. Values of the Surface Free Energy and its components calculated according to vOCG approach for active and support layers of the CTA membrane.

	ACTIVE LAYER [mJ/m^2]						SUPPORT LAYER [mJ/m^2]				
	γ^{TOT}	γ^{AB}	γ^{LW}	γ^+	γ^-		γ^{TOT}	γ^{AB}	γ^{LW}	γ^+	γ^-
clean	30.52	0.41	30.11	0.17	0.26	**clean**	35.41	0.73	34.67	0.23	0.58
fouled	31.99	5.88	26.10	0.30	29.31	**fouled**	39.43	0.34	39.09	0.00	15.26

4. Conclusions

Results from this study demonstrate the FO process as a promising method for concentration of AKG. The initial pH of the FS is an important parameter affecting mainly AKG rejection. AKG rejection increased with increasing initial pH of the feed solution. The highest AKG rejection value of 99.7% was achieved at pH 5~~(99.7% at initial pH value equal to 5).~~ The use of the FO process allowed for a high water recovery of 80% and corresponding 2-fold concentration of the AKG, even when real fermentation broth was used as the FS. On the other hand, the water flux at 80% water recovery was strongly dependent on the composition of the FS, which can be observed in the concentration of actual post-fermentation broth. The fouling analyzes suggested that fouling after the FO process for obtaining AKG from the fermentation broth could be relatively reversible. The development of the integrated membrane process to purify AKG from the post-fermentation broth is a promising approach. However, the limitations due to fouling

need to be considered and resolved for the further practical application. Moreover, the selection of the easiest but still effective pretreatment is possibly one of the key factors of the successful process.

5. Acknowledgements

The article was created thanks to participation in program PROM of the Polish National Agency for Academic Exchange. The program is co-financed from the European Social Fund within the Operational Program Knowledge Education Development, non-competitive project entitled "International scholarship exchange of PhD students and academic staff" executed under the Activity 3.3 specified in the application for funding of project No. POWR.03.03.00-00-PN13/18. Lei Zheng would like to thank Faculty of Engineering and Information Technology (FEIT), University of Technology Sydney (UTS) for awarding him a FEIT PhD Post-Thesis Publication Award. He also appreciates China Scholarship Council and UTS for the provision of a doctoral scholarship.

6. References

[1] W. Zeng, H. Zhang, S. Xu, F. Fang, J. Zhou, Biosynthesis of keto acids by fed-batch culture of Yarrowia lipolytica WSH-Z06, Bioresour. Technol. 243 (2017) 1037–1043. doi:10.1016/j.biortech.2017.07.063.

[2] B. Tugnoli, G. Giovagnoni, A. Piva, E. Grilli, From acidifiers to intestinal health enhancers: How organic acids can improve growth efficiency of pigs, Animals. 10 (2020) 1–18. doi:10.3390/ani10010134.

[3] L. Liu, Systems and Synthetic Biotechnology for Production of Nutraceuticals, 2019. doi:10.1007/978-981-15-0446-4.

[4] S. V. Kamzolova, M.N. Chiglintseva, J.N. Lunina, I.G. Morgunov, α-Ketoglutaric acid production by Yarrowia lipolytica and its regulation, Appl. Microbiol. Biotechnol. 96 (2012) 783–791. doi:10.1007/s00253-012-4222-x.

[5] C. Otto, V. Yovkova, A. Aurich, S. Mauersberger, G. Barth, Variation of the by-product spectrum during a-ketoglutaric acid production from raw glycerol by overexpression of fumarase and pyruvate carboxylase genes in Yarrowia lipolytica, Appl. Microbiol. Biotechnol. 95 (2012) 905–917. doi:10.1007/s00253-012-4085-1.

[6] J.W. Paulina Grzesiak, Monika Słupecka-Ziemilska, The Biological Role of Alpha-

452 Ketoglutaric Acid in Physiological Processes and Its Therapeutic Potential, Dev. Period
453 Med. XX (2016) 61–67.

454 [7] A. Rywińska, L. Tomaszewska-Hetman, M. Rakicka-Pustułka, P. Juszczyk, W.
455 Rymowicz, Alpha-ketoglutaric acid production from a mixture of glycerol and rapeseed
456 oil by Yarrowia lipolytica using different substrate feeding strategies, Sustain. 12 (2020).
457 doi:10.3390/su12156109.

458 [8] Z. Luo, S. Yu, W. Zeng, J. Zhou, Comparative analysis of the chemical and biochemical
459 synthesis of keto acids, Biotechnol. Adv. 47 (2021) 107706.
460 doi:10.1016/j.biotechadv.2021.107706.

461 [9] D.G. Barrett, M.N. Yousaf, Design and applications of biodegradable polyester tissue
462 scaffolds based on endogenous monomers found in human metabolism, Molecules. 14
463 (2009) 4022–4050. doi:10.3390/molecules14104022.

464 [10] M. Szczygiełda, K. Prochaska, Effective separation of bio-based alpha-ketoglutaric acid
465 from post-fermentation broth using bipolar membrane electrodialysis (EDBM) and
466 fouling analysis, Biochem. Eng. J. 166 (2020) 1–10. doi:10.1016/j.bej.2020.107883.

467 [11] H. Guo, S. Su, C. Madzak, J. Zhou, H. Chen, G. Chen, Applying pathway engineering
468 to enhance production of alpha-ketoglutarate in Yarrowia lipolytica, Appl. Microbiol.
469 Biotechnol. 100 (2016) 9875–9884. doi:10.1007/s00253-016-7913-x.

470 [12] A. Rywińska, P. Juszczyk, M. Wojtatowicz, M. Robak, Z. Lazar, L. Tomaszewska, W.
471 Rymowicz, Glycerol as a promising substrate for Yarrowia lipolytica biotechnological
472 applications, Biomass and Bioenergy. 48 (2013) 148–166.
473 doi:10.1016/j.biombioe.2012.11.021.

474 [13] M. Szczygiełda, K. Prochaska, Downstream separation and purification of bio-based
475 alpha-ketoglutaric acid from post-fermentation broth using a multi-stage membrane
476 process, Process Biochem. 96 (2020) 38–48. doi:10.1016/j.procbio.2020.05.026.

477 [14] J. Antczak, M. Szczygiełda, K. Prochaska, Nanofiltration separation of succinic acid
478 from post-fermentation broth: Impact of process conditions and fouling analysis, J. Ind.
479 Eng. Chem. 77 (2019) 253–261. doi:10.1016/j.jiec.2019.04.046.

480 [15] A. Krzyżkowska, M. Regel-rosocka, The effect of fermentation broth composition on
481 removal of carboxylic acids by reactive extraction with Cyanex 923, Sep. Purif. Technol.

236 (2020) 116289. doi:10.1016/j.seppur.2019.116289.

[16] Q. Li, D. Wang, Y. Wu, W. Li, Y. Zhang, J. Xing, Z. Su, One step recovery of succinic acid from fermentation broths by crystallization, Sep. Purif. Technol. 72 (2010) 294–300. doi:10.1016/j.seppur.2010.02.021.

[17] B. Rukowicz, K. Alejski, Separation and Puri fi cation Technology A biologically-derived 1 , 3-propanediol recovery from fermentation broth using preparative liquid chromatography, Sep. Purif. Technol. 205 (2018) 196–202. doi:10.1016/j.seppur.2018.05.041.

[18] N.T.H. Thuy, A. Boontawan, Production of very-high purity succinic acid from fermentation broth using microfiltration and nanofiltration-assisted crystallization, J. Memb. Sci. 524 (2017) 470–481. doi:10.1016/j.memsci.2016.11.073.

[19] C.J. Davey, A. Havill, D. Leak, D.A. Patterson, Nanofiltration and reverse osmosis membranes for purification and concentration of a 2,3-butanediol producing gas fermentation broth, J. Memb. Sci. 518 (2016) 150–158. doi:10.1016/j.memsci.2016.06.044.

[20] P. Dey, L. Linnanen, P. Pal, Separation of lactic acid from fermentation broth by cross flow nanofiltration: Membrane characterization and transport modelling, Desalination. 288 (2012) 47–57. doi:10.1016/j.desal.2011.12.009.

[21] M.J. Woźniak, K. Prochaska, Fumaric acid separation from fermentation broth using nanofiltration (NF) and bipolar electrodialysis (EDBM), Sep. Purif. Technol. 125 (2014) 179–186. doi:10.1016/j.seppur.2014.01.051.

[22] M. Szczygiełda, K. Prochaska, Alpha-ketoglutaric acid production using electrodialysis with bipolar membrane, J. Memb. Sci. 536 (2017) 37–43. doi:10.1016/j.memsci.2017.04.059.

[23] H.G. Zeweldi, L.A. Limjuco, A.P. Bendoy, H.S. Kim, M.J. Park, H.K. Shon, E.M. Johnson, H. Lee, W.J. Chung, G.M. Nisola, The potential of monocationic imidazolium-, phosphonium-, and ammonium-based hydrophilic ionic liquids as draw solutes for forward osmosis, Desalination. 444 (2018) 94–106. doi:10.1016/j.desal.2018.07.017.

[24] P. Menchik, C.I. Moraru, Nonthermal concentration of liquid foods by a combination of reverse osmosis and forward osmosis. Acid whey: A case study, J. Food Eng. 253 (2019)

512 40–48. doi:10.1016/j.jfoodeng.2019.02.015.

513 [25] X. An, Y. Hu, N. Wang, Z. Zhou, Z. Liu, Continuous juice concentration by integrating
514 forward osmosis with membrane distillation using potassium sorbate preservative as a
515 draw solute, J. Memb. Sci. 573 (2019) 192–199. doi:10.1016/j.memsci.2018.12.010.

516 [26] M. Vu, L.N. Nguyen, M.A. Hasan Johir, X. Zhang, L.D. Nghiem, M. Elimelech, Biogas
517 sparging to control fouling and enhance resource recovery from anaerobically digested
518 sludge centrate by forward osmosis, J. Memb. Sci. 625 (2021) 119176.
519 doi:10.1016/j.memsci.2021.119176.

520 [27] N.T. Hau, S.S. Chen, N.C. Nguyen, K.Z. Huang, H.H. Ngo, W. Guo, Exploration of
521 EDTA sodium salt as novel draw solution in forward osmosis process for dewatering of
522 high nutrient sludge, J. Memb. Sci. 455 (2014) 305–311.
523 doi:10.1016/j.memsci.2013.12.068.

524 [28] G. Chen, Z. Wang, L.D. Nghiem, X.M. Li, M. Xie, B. Zhao, M. Zhang, J. Song, T. He,
525 Treatment of shale gas drilling flowback fluids (SGDFs) by forward osmosis: Membrane
526 fouling and mitigation, Desalination. 366 (2015) 113–120.
527 doi:10.1016/j.desal.2015.02.025.

528 [29] J.Y. Law, A.W. Mohammad, Z.K. Tee, N.K. Zaman, J.M. Jahim, J. Santanaraj, M.S.
529 Sajab, Recovery of succinic acid from fermentation broth by forward osmosis-assisted
530 crystallization process, J. Memb. Sci. 583 (2019) 139–151.
531 doi:10.1016/j.memsci.2019.04.036.

532 [30] S. Zhao, L. Zou, C.Y. Tang, D. Mulcahy, Recent developments in forward osmosis:
533 Opportunities and challenges, J. Memb. Sci. 396 (2012) 1–21.
534 doi:10.1016/j.memsci.2011.12.023.

535 [31] J. Garcia-Aguirre, M. Alvarado-Morales, I.A. Fotidis, I. Angelidaki, Up-concentration
536 of succinic acid, lactic acid, and ethanol fermentations broths by forward osmosis,
537 Biochem. Eng. J. 155 (2020) 107482. doi:10.1016/j.bej.2019.107482.

538 [32] G. Blandin, B. Rosselló, V.M. Monsalvo, P. Batlle-Vilanova, J.M. Viñas, F. Rogalla, J.
539 Comas, Volatile fatty acids concentration in real wastewater by forward osmosis, J.
540 Memb. Sci. 575 (2019) 60–70. doi:10.1016/j.memsci.2019.01.006.

541 [33] J.Y. Law, A.W. Mohammad, Multiple-solute salts as draw solution for osmotic

concentration of succinate feed by forward osmosis, J. Ind. Eng. Chem. (2017). doi:10.1016/j.jiec.2017.03.011.

[34] J.Y. Law, A.W. Mohammad, Osmotic concentration of succinic acid by forward osmosis: Influence of feed solution pH and evaluation of seawater as draw solution, Chinese J. Chem. Eng. 26 (2018) 976–983. doi:10.1016/j.cjche.2017.10.003.

[35] S.J. Im, G. Jeong, S. Jeong, J. Cho, A. Jang, Fouling and transport of organic matter in cellulose triacetate forward-osmosis membrane for wastewater reuse and seawater desalination, Chem. Eng. J. 384 (2020) 123341. doi:10.1016/j.cej.2019.123341.

[36] K. Jung, J.D.R. Choi, D. Lee, C. Seo, J. Lee, S.Y. Lee, H.N. Chang, Y.C. Kim, Permeation characteristics of volatile fatty acids solution by forward osmosis, Process Biochem. 50 (2015) 669–677. doi:10.1016/j.procbio.2015.01.016.

[37] J. Feher, Osmosis and Osmotic Pressure, in: Quant. Hum. Physiol., 2012: pp. 141–152. doi:10.1016/b978-0-12-382163-8.00017-7.

[38] J. Shan, W.A. Phillip, M. Elimelech, Coupled reverse draw solute permeation and water flux in forward osmosis with neutral draw solutes, 393 (2012) 9–17. doi:10.1016/j.memsci.2011.11.020.

[39] H. Xu, K. Xiao, X. Wang, S. Liang, C. Wei, X. Wen, Outlining the Roles of Membrane-Foulant and Foulant-Foulant Interactions in Organic Fouling During Microfiltration and Ultrafiltration : A Mini-Review, Front. Chem. 8 (2020) 1–14. doi:10.3389/fchem.2020.00417.

[40] G. Blandin, H. Vervoort, P. Le-clech, A.R.D. Verliefde, Journal of Water Process Engineering Fouling and cleaning of high permeability forward osmosis membranes, J. Water Process Eng. 9 (2016) 161–169. doi:10.1016/j.jwpe.2015.12.007.

[41] M.M. Motsa, B.B. Mamba, A.D. Haese, E.M. V Hoek, A.R.D. Verliefde, Organic fouling in forward osmosis membranes : The role of feed solution chemistry and membrane structural properties, J. Memb. Sci. 460 (2014) 99–109. doi:10.1016/j.memsci.2014.02.035.

[42] L. Feng, X. Li, G. Du, J. Chen, Adsorption and fouling characterization of Klebsiella oxytoca to microfiltration membranes, 44 (2009) 1289–1292. doi:10.1016/j.procbio.2009.07.017.

572 [43] N. Subhi, A.R.D. Verliefde, V. Chen, P. Le-Clech, Assessment of physicochemical
573 interactions in hollow fibre ultrafiltration membrane by contact angle analysis, J. Memb.
574 Sci. 403–404 (2012) 32–40. doi:10.1016/j.memsci.2012.02.007.

575

576 7. Supplementary materials

577 Table SM1. CTA membrane parameters based on the manufacturers data and own
578 measurements (marked with *)

membrane parameter	value
manufacturer	Sterlitech, FTS H2O
polymer	cellulose triacetate (CTA)
operating temperature	5-50°C
pH range	3-7
short term exposure pH range	2-11
minimum transmembrane pressure	5 psi
maximum inlet pressure	75 psi
water flux	>7 L/m^2/h (H_2O vs. 1 M NaCl; FO mode)
NaCl reverse flux	<2 L/m^2/h (H_2O vs. 1 M NaCl; FO mode)
thickness	110 micron (±15 micron)
average roughness*	65 nm (by AFM)

579

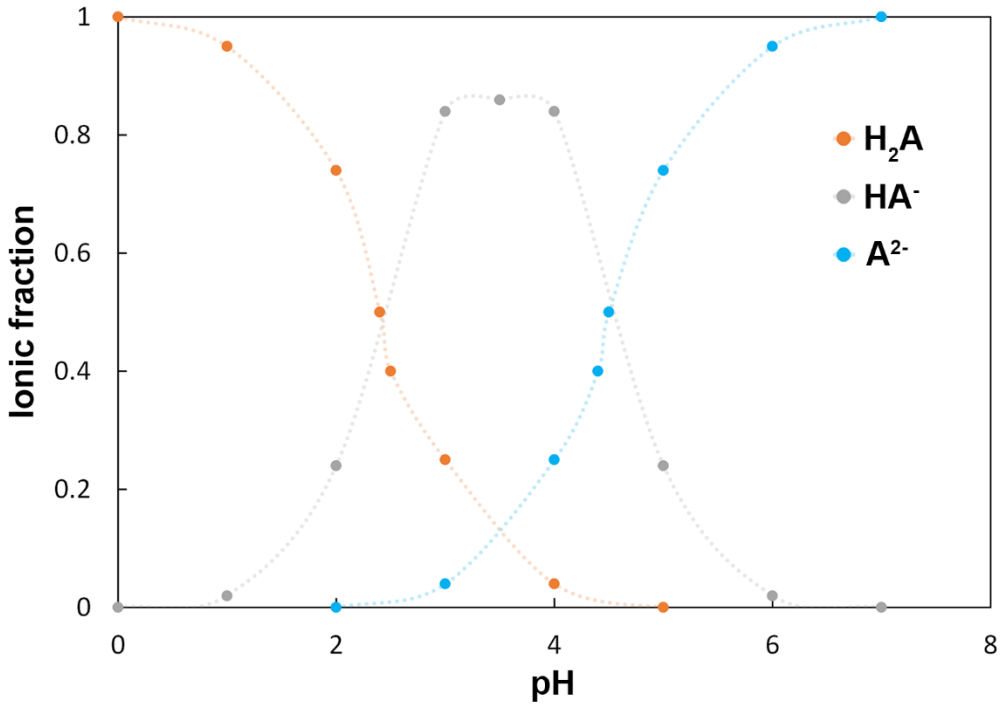

580

581 Fig. SM1. Change of the AKG ionic fraction in the function of pH.

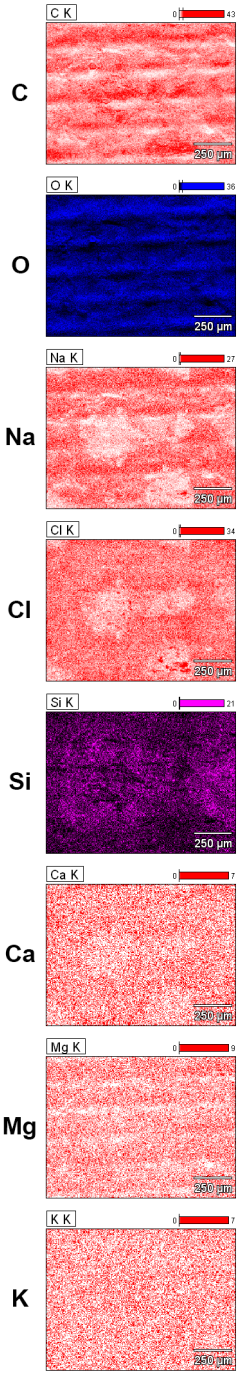

582

583 Fig. SM2. Distribution of the elements on the sample of fouled membrane from EDS.

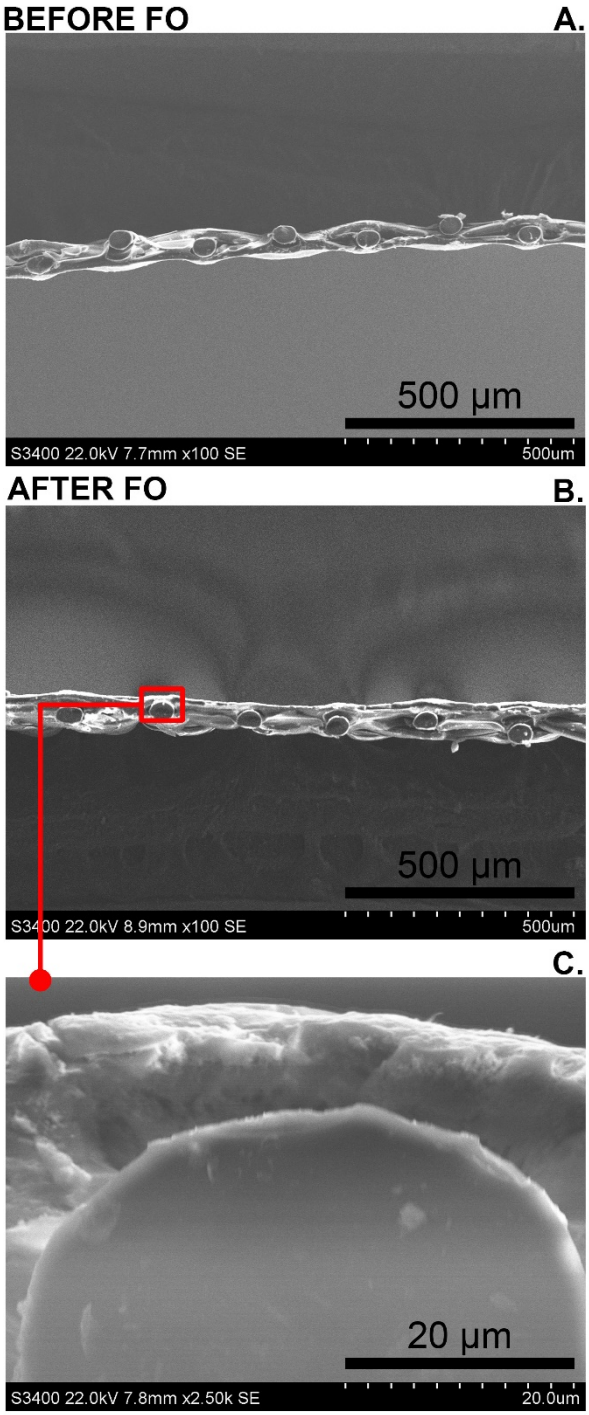

584

585 Fig. SM3. SEM images – cross-sections of virgin CTA membrane (A) and membrane fouled
586 with real broth, at various magnification (B-C).

587

588

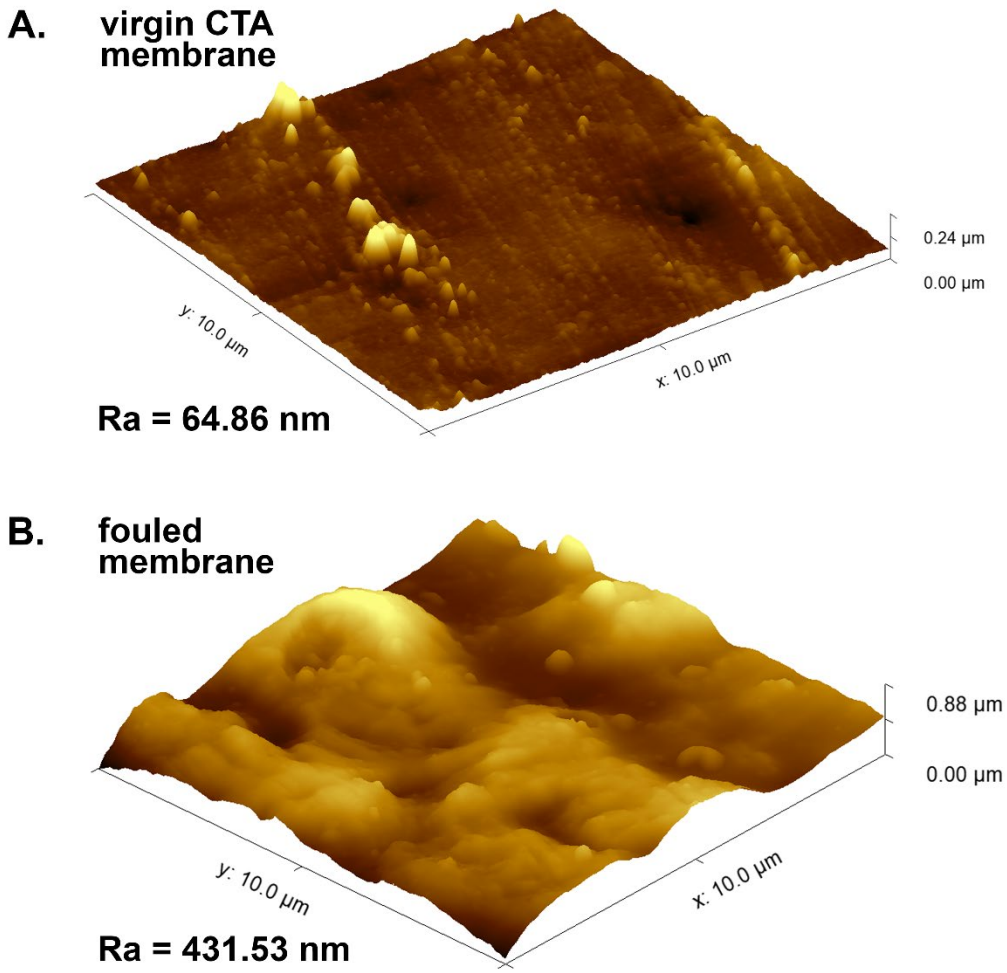

589

590 Fig. SM4. AFM micrographs of the virgin CTA membrane (A) and fouling cake layer of the
591 real fermentation broth (B) with roughness values.

592